



**HAL**  
open science

# Electrically silent divalent cation entries in resting and active voltage-controlled muscle fibers.

Céline Berbey, Bruno Allard

► **To cite this version:**

Céline Berbey, Bruno Allard. Electrically silent divalent cation entries in resting and active voltage-controlled muscle fibers.. *Biophysical Journal*, 2009, 96 (7), pp.2648-57. 10.1016/j.bpj.2009.01.008 . hal-00387458

**HAL Id: hal-00387458**

**<https://hal.science/hal-00387458>**

Submitted on 25 May 2009

**HAL** is a multi-disciplinary open access archive for the deposit and dissemination of scientific research documents, whether they are published or not. The documents may come from teaching and research institutions in France or abroad, or from public or private research centers.

L'archive ouverte pluridisciplinaire **HAL**, est destinée au dépôt et à la diffusion de documents scientifiques de niveau recherche, publiés ou non, émanant des établissements d'enseignement et de recherche français ou étrangers, des laboratoires publics ou privés.

# **Electrically silent divalent cation entries in resting and active voltage-controlled muscle fibers**

**Céline BERBEY and Bruno ALLARD**

Physiologie Intégrative Cellulaire et Moléculaire, Université Lyon 1, CNRS UMR 5123, Villeurbanne, France

**Running title:**  $Mn^{2+}$  entry and current in muscle cells

**Keywords:** calcium influx,  $Mn^{2+}$  quenching of fura-2 fluorescence, voltage clamp, action potential, L-type channels, excitation-contraction coupling.

## **Abstract**

$\text{Ca}^{2+}$  is known to enter skeletal muscle at rest and during activity. Except for the well characterized  $\text{Ca}^{2+}$  entry through L-type channels, pathways involved in these  $\text{Ca}^{2+}$  entries remain elusive in adult muscle. This study investigates  $\text{Ca}^{2+}$  influx at rest and during activity using the method of  $\text{Mn}^{2+}$  quenching of fura-2 fluorescence on voltage-controlled adult skeletal muscle cells. Resting rate of  $\text{Mn}^{2+}$  influx depended on external  $[\text{Mn}^{2+}]$  and membrane potential. At -80 mV, replacement of  $\text{Mg}^{2+}$  by  $\text{Mn}^{2+}$  gave rise to an outward current associated with an increase in cell input resistance. Calibration of fura-2 response indicated that  $\text{Mn}^{2+}$  influx was too small to be resolved as a macroscopic current. Partial depletion of the sarcoplasmic reticulum induced by a train of action potentials in the presence of cyclopiazonic acid led to a slight increase in resting  $\text{Mn}^{2+}$  influx but no change in cell input resistance and membrane potential. Trains of action potentials considerably increased  $\text{Mn}^{2+}$  entry through an electrically silent pathway independent of L-type channels which provided 24% of the global  $\text{Mn}^{2+}$  influx at +30 mV under voltage-clamp conditions. Within this context, the nature and the physiological role of the  $\text{Ca}^{2+}$  pathways involved during muscle excitation still remain open questions.

## Introduction

In skeletal muscle,  $\text{Ca}^{2+}$  ions triggering contraction are released from the sarcoplasmic reticulum (SR) in response to depolarization of the cell. In parallel to these massive variations of intracellular  $\text{Ca}^{2+}$ , a  $\text{Ca}^{2+}$  influx is also known to occur through the sarcolemma both in resting and working muscle.

Early measurements using radiolabelled  $\text{Ca}^{2+}$  have shown that  $\text{Ca}^{2+}$  slowly enters skeletal muscle cells in resting conditions (1). The physiological role of this  $\text{Ca}^{2+}$  entry is poorly understood in normal muscle but several lines of evidence suggest that a chronic elevation of the resting influx of  $\text{Ca}^{2+}$  might contribute to the initiation or progression of muscle cell degeneration in a number of muscle disorders (2). Within this context of potential pathophysiological consequences of exacerbated  $\text{Ca}^{2+}$  entry, the study of resting  $\text{Ca}^{2+}$  influx and the search for the pathways through which it takes place are of fundamental interest. A widespread hypothesis suggests that  $\text{Ca}^{2+}$  enters resting muscle cell through ion channels. Single channel recordings indeed revealed opening of poorly selective cation channels carrying inward current at negative membrane potentials in isolated mouse skeletal muscle fibers (3-6). However, subsarcolemmal  $\text{Ca}^{2+}$  load revealed by the measurement of  $\text{Ca}^{2+}$ -activated  $\text{K}^+$  channel opening was found to be independent of the activity of the spontaneously active  $\text{Ca}^{2+}$  channels suggesting the existence of electrically silent sites of passive  $\text{Ca}^{2+}$  influx (7). Additionally, certainly because of the absence of specific inhibitors of  $\text{Ca}^{2+}$  channels active at rest and because of the drastic modifications of the electrophysiological muscle properties resulting from manipulation of external  $\text{Ca}^{2+}$ , there is no experimental evidence available demonstrating the development of a  $\text{Ca}^{2+}$  current at the whole cell level under resting conditions.

Another way to monitor  $\text{Ca}^{2+}$  influx at rest is to measure the changes in fluorescence of  $\text{Ca}^{2+}$  dyes. Early works investigating plasmalemmal divalent cations influx in non-excitabile cells have introduced the use of  $\text{Mn}^{2+}$  as a surrogate of  $\text{Ca}^{2+}$  to directly assess  $\text{Ca}^{2+}$  entry (e.g. 8).  $\text{Mn}^{2+}$  ions are assumed to penetrate cells through the same pathways as the ones used by  $\text{Ca}^{2+}$  and, once within the cells, these ions are trapped in the cytosol and strongly quench the fluorescence emitted by  $\text{Ca}^{2+}$  dyes. In adult skeletal muscle, this  $\text{Mn}^{2+}$  quenching method has been used to confirm that the muscle sarcolemma has a substantial permeability to divalent cations under resting conditions but they were performed in the absence of voltage control and therefore did not establish whether  $\text{Mn}^{2+}$  entry generated a measurable macroscopic membrane current whose properties could give evidence for the existence of ion channels open at rest, permeable to  $\text{Mn}^{2+}$  and  $\text{Ca}^{2+}$  (e.g. 9). The  $\text{Mn}^{2+}$  quenching method has also been used to show that SR depletion induced in the presence of SR  $\text{Ca}^{2+}$ -ATPase inhibitors gave rise to an increase in resting  $\text{Ca}^{2+}$  influx in adult and fetal muscle fibers (10, 11). However, using voltage clamp on adult muscle fibers, Allard *et al.* (12) demonstrated that SR depletion was not associated with the generation of a resting inward current thus challenging the physiological relevance of a store-operated membrane conductance in adult skeletal muscle.

In working adult muscle, depolarization elicits a well characterized  $\text{Ca}^{2+}$  entry through L-type  $\text{Ca}^{2+}$  channels early recorded as a voltage-activated current. But more recently, using the  $\text{Mn}^{2+}$  quenching method in primary myotubes, Cherednichenko *et al.* (13) demonstrated that membrane depolarization initiated a  $\text{Ca}^{2+}$  entry independent of the voltage-gated L-type  $\text{Ca}^{2+}$  current and of SR depletion. An increased  $\text{Ca}^{2+}$  entry provoked by KCl depolarization was also recently described in adult muscle (14), but there was no attempt to determine if this  $\text{Ca}^{2+}$  entry was independent of the voltage-activated L-type  $\text{Ca}^{2+}$  current as found in myotubes. There is also no available information about the behaviour of this  $\text{Ca}^{2+}$  influx as a function of the membrane voltage which is yet recognized to tightly control  $\text{Ca}^{2+}$  changes in skeletal muscle.

The present study is the first to combine the  $Mn^{2+}$  quenching method and voltage control on adult mouse skeletal muscle cell to investigate sarcolemmal  $Ca^{2+}$  influx under resting and active conditions. Monitoring of the background membrane current during  $Mn^{2+}$  influx together with calibration of the fura-2 response to  $Mn^{2+}$  led us to conclude that the  $Mn^{2+}$  influx at rest and in response to partial depletion of the SR does not induce any resolvable macroscopic current. We also demonstrate that the rate of  $Mn^{2+}$  entry is markedly increased by tetanic muscle activity principally through an electrically silent voltage-dependent  $Ca^{2+}$  entry independent of the voltage activated L-type current.

## **Materials and methods**

### ***Preparation of muscle fibers***

Experiments were performed on single skeletal fibers enzymatically isolated from interosseal muscles of adult male Swiss OF1 mice. All experiments were performed in accordance with the guidelines of the French Ministry of Agriculture (87/848) and of the European Community (86/609/EEC). Procedures for enzymatic isolation of single muscle fibers and partial insulation of the fibers with silicone grease were as described previously (15). In brief, the major part of a single fiber (between 0.5 and 1 mm length) was electrically insulated with silicone grease so that a fiber portion between 50 and 100  $\mu m$  length was left free of grease. A micropipette was then inserted into the fiber through the silicone layer. Under these conditions, whole-cell voltage clamp could be achieved on the portion of the fiber extremity free of grease. The tip of the micropipette was then crushed into the dish bottom to allow intracellular dialysis of the fiber (16).

### ***Electrophysiology***

Fibers were voltage clamped with an RK-400 patch-clamp amplifier (Bio-Logic, Claix, France) used in the whole-cell configuration. Command voltage pulse generation and data acquisition were done using the pClamp10 software (Axon Instruments Inc., USA) driving an A/D converter (Digidata 1322A, Axon Instruments Inc., USA). Analog compensation was systematically used to decrease the effective series resistance. Voltage-clamp was performed with a microelectrode filled with the whole-cell intra-pipette solution (see Solutions). Cell capacitance was determined by integration of a current trace obtained with a 10-mV hyperpolarizing pulse from the holding potential and used to calculate the density of  $Mn^{2+}$  currents (A/F). For voltage activated currents, leak currents were subtracted from all recordings using a 10-mV hyperpolarizing pulse preceding every test pulse from the holding potential supposing a linear evolution of leak current with depolarization. The voltage dependence of the mean  $Mn^{2+}$  current density was fitted using the following equation:  $I(V) = G_{max} (V - V_{rev}) / ((1 + \exp((V_{0.5} - V)/k)))$ , where  $I(V)$  is the mean density of the current measured,  $V$  the test pulse,  $G_{max}$  the maximum conductance,  $V_{rev}$  the apparent reversal potential,  $V_{0.5}$  the half-activation voltage and  $k$  a steepness factor. The voltage dependence of the normalized conductance was obtained by dividing  $I(V)$  by  $G_{max}(V - V_{rev})$ .

### ***$Mn^{2+}$ quenching experiments***

Prior to experiments, cells were dialysed during 20 minutes with an internal pipette solution containing 100  $\mu M$  fura-2 (see Preparation of muscle fibers) and imaged with an inverted microscope (Nikon Diaphot) equipped for epifluorescence using a 40x oil-immersion objective. Fura-2 fluorescence was measured with monochromatic excitation at a  $Ca^{2+}$ -insensitive wavelength (360 nm) (T.I.L.L. Photonics, Martinsried, Germany). Images from a circular region of 20  $\mu m$  diameter centred on the silicone-free extremity of the cell under study were captured with a Darkstar 800 device camera (Photonic Science, Robertsbridge,

UK) at a frequency of 0.2 Hz or 0.1 Hz. This low sampling rate was chosen so that cells were exposed to the excitation beam very shortly (200 ms) during image capture to make photo-bleaching negligible. Image acquisition and processing were performed using the Axon Imaging Workbench (Axon Instruments Inc., USA). Fluorescence values were expressed as percentage of the initial fluorescence recorded before addition of  $Mn^{2+}$  to the external medium, corrected for background fluorescence. Under resting conditions, the rate of fluorescence quenching was determined by fitting a linear regression to the fluorescence records. In response to a train of action potentials (AP) or to voltage pulses, given the low image acquisition frequency, the  $Mn^{2+}$  influx rate was extrapolated from the absolute decrease in fluorescence between two fluorescence data points.

### ***In vitro and in vivo calibration of $Mn^{2+}$ quenching***

For *in vitro* calibration, the fura-2 fluorescence was measured on pulled glass tubes of 50  $\mu m$  internal diameter filled with an aqueous solution containing 100  $\mu M$  fura-2 and various  $[MnCl_2]$ . For *in vivo* calibration, cells dialyzed with an internal solution containing 100  $\mu M$  fura-2 were exposed to a solution containing (in mM) 140 K-glutamate, 10 HEPES adjusted to pH 7.2 with K-OH and 20  $\mu M$  ionomycin. Increasing concentrations of  $MnCl_2$  were added in this external solution and the fura-2 fluorescence was measured after fluorescence intensity had reached a new steady state.

### ***Estimation of $Mn^{2+}$ current intensity on the basis of $Mn^{2+}$ quenching rates***

The membrane surface area was estimated by measuring the capacitance of the portion of the cell under study and assuming a specific capacitance of 4.5  $\mu F.cm^{-2}$  (17). This surface value was used to estimate the cell volume into which  $Mn^{2+}$  diluted once within the cell assuming an average cell diameter of 40  $\mu m$ . The quenching rate ( $\%.min^{-1}$ ) recorded in every cell was then converted into intracellular  $Mn^{2+}$  concentration reached after one minute using the relationship obtained between the relative fluorescence intensity emitted by the fibers and the external concentration of  $Mn^{2+}$  in the presence of ionomycin (see above and Fig. 4). This gave the quantity of divalent charges accumulated in the calculated cell volume after one minute which in turn, divided by 60 and by the value of cell capacitance, yielded the density of  $Mn^{2+}$  current that should have flowed through the sarcolemma.

### ***Solutions***

For experiments in relation with Fig. 1, 5B, C and 7C, the external saline corresponded to a standard Tyrode solution containing (in mM) 140 NaCl, 5 KCl and 10 HEPES adjusted to pH 7.2 with NaOH with no added  $Ca^{2+}$  and various concentrations of  $MgCl_2$ .  $MgCl_2$  was replaced by  $MnCl_2$  at equimolar concentrations to minimize surface charge effects. For experiments in relation with Fig. 5A, 1 mM  $MnCl_2$  was added in a Tyrode solution containing 2 mM  $CaCl_2$  and 2 mM  $MgCl_2$ . For experiments in relation with Fig. 2, 3, 6, 7A, B and D, the external solution contained (in mM) 140 TEA-methanesulfonate, 10 HEPES adjusted to pH 7.2 with TEA-OH with no added  $Ca^{2+}$  and various concentrations of  $MgCl_2$ .  $MgCl_2$  was replaced by  $MnCl_2$  at equimolar concentrations. For experiments in relation with Fig. 6 and 7A, 1.5 mM 4-aminopyridine was added in the external solution. The whole-cell intra-pipette solution contained (in mM) 120 K-glutamate, 5  $Na_2$ -ATP, 5  $Na_2$ -phosphocreatine, 5.5  $MgCl_2$ , 5 glucose, 5 HEPES adjusted to pH 7.2 with K-OH except for experiments in relation with Fig. 3 where the intra-pipette solution contained (in mM) 120 Cs-aspartate, 5  $Na_2$ -ATP, 5.5  $MgCl_2$ , 5 glucose, 0.1 EGTA, 5 HEPES adjusted to pH 7.2 with Cs-OH. Fura-2 was dissolved in water at 10 mM, cyclopiazonic acid (CPA), 9-anthracene carboxylic acid (9AC) and ionomycin were dissolved in dimethylsulfoxide at 50 mM, 100 mM and 1 mM respectively and diluted to the required concentration in the solutions. Cells were exposed to different

solutions by placing them in the mouth of a perfusion tube from which flowed by gravity the rapidly exchanged solutions. Experiments were carried out at room temperature.

### **Statistics**

Least-squares fits were performed using a Marquardt-Levenberg algorithm routine included in Microcal Origin (Microcal Software Inc., Northampton, MA). Data are given as means  $\pm$  S.E.M and compared using unpaired, paired *t*-tests or ANOVA as indicated in the text. Differences were considered significant when  $P < 0.05$ .

## **Results**

### **Divalent cation influx at rest**

Figure 1 illustrates the quenching of fura-2 fluorescence in fibers voltage-clamped at -80 mV in response to the addition of various concentrations of  $Mn^{2+}$  in  $Ca^{2+}$ -free external solutions. Replacement of 3 mM  $Mg^{2+}$  by 3 mM  $Mn^{2+}$  in the external solution induced a marked reduction of the fura-2 fluorescence which remained at a stabilized lower value upon removal of  $Mn^{2+}$  (Fig. 1A). As long as the fluorescence signal remained higher than 50 % of its initial value, it declined linearly with time so that the rate of quenching could be estimated by fitting the fluorescence decline with a linear regression. Fig. 1B shows that the rate of fluorescence decline was dependent on the external  $[Mn^{2+}]$ . On average, an elevation of the external concentration of  $Mn^{2+}$  induced a significant gradual increase in the rate of quenching (Fig. 1C) ( $P = 0.0075$ , ANOVA). When 2 mM  $Ca^{2+}$  was added to a 10 mM  $Mn^{2+}$  containing Tyrode solution, the rate of quenching was approximately reduced by half ( $P = 0.02$ , unpaired *t*-test).

A second set of experiments was performed in order to determine how the rate of quenching was affected by the membrane potential. To improve the control of the membrane potential, cells were bathed in an external solution containing 140 mM TEA-methanesulfonate. Figure 2A presents the drop of fluorescence induced by replacement of 3 mM external  $Mg^{2+}$  by  $Mn^{2+}$  in four different cells held at +40, 0, -40 or -80 mV. On average, Fig. 2B shows that the less negative the membrane potential, the lower the rate of quenching ( $P = 0.019$ , ANOVA). The effect of a change in membrane potential on the rate of  $Mn^{2+}$  quenching could also be revealed on a same fiber. A hyperpolarization of 60 mV amplitude indeed induced an increase of the rate of quenching but which depended on the initial value of the holding potential (Fig. 2C). Figure 2D clearly illustrates that in average the more depolarized the initial holding potential, the lower the factor of increase of the quenching rate induced by the 60-mV negative voltage step.

### **Membrane current associated with resting cation influx**

We next tried to determine if the influx of  $Mn^{2+}$  ion responsible for the quenching of fura-2 fluorescence was associated with a measurable macroscopic inward current. Figure 3A shows that, at a holding potential of -80 mV, replacement of 3 mM  $Mg^{2+}$  by  $Mn^{2+}$  led to the development of an outward current associated with the quenching of fluorescence. In another cell held at +40 mV, the same manoeuvre gave rise to an inward current associated with a lower rate of quenching of fluorescence (Fig. 3B). The same respective behaviours were observed in 10 fibers tested at -80 mV and in 7 fibers tested at +40 mV. In order to determine whether the outward current which developed at -80 mV in response to replacement of  $Mg^{2+}$  by  $Mn^{2+}$  resulted from the opening or closing of ion channels, the input resistance was challenged by applying every 5 s voltage ramps bringing the holding potential from -40 to -100 mV. To minimize the contribution of  $Cl^-$  and  $K^+$  channels, cells were dialyzed with a Cs-aspartate containing solution and the  $Cl^-$  blocker 9AC was added in the TEA-

methanesulfonate containing external solution. Also, 10 mM  $Mg^{2+}$  was replaced by 10 mM  $Mn^{2+}$  to strengthen the inwardly directed  $Mn^{2+}$  concentration gradient. Figures 3C and D show that replacement of  $Mg^{2+}$  by  $Mn^{2+}$  gave rise to a robust and reversible outward current associated with a decrease in the cell electrical conductance as evidenced by the decrease in the slope of the current induced by the voltage ramp. In 8 cells tested, the density of the inward background current at -80 mV was reduced from  $3.13 \pm 0.32$  to  $2.65 \pm 0.26$  A/F while the cell conductance was reduced from  $50 \pm 5$  to  $43 \pm 4$  S/F upon replacement of  $Mg^{2+}$  by  $Mn^{2+}$  which both represent a  $14.6 \pm 1.8$  % decrease ( $P < 0.001$ , paired  $t$ -test). This result indicates that the main effect of external  $Mn^{2+}$  is to block spontaneously active ion channels carrying inward currents at -80 mV rather to open channels carrying outward currents. It has to be mentioned that lower  $Mn^{2+}$  concentrations (1 mM or 100  $\mu$ M) which, as expected, induced a weaker blocking effect but concomitantly reduced the  $Mn^{2+}$  concentration gradient, never elicited any discernable inward current at negative membrane potentials (not shown). The nature of the ion channels blocked by  $Mn^{2+}$  was not further investigated.

Another possible interpretation of these results is that the inward current generated by the  $Mn^{2+}$  entry is too minute to be resolved under voltage clamp conditions and may be masked by a predominant blocking effect of  $Mn^{2+}$  on resting conductances. To address this question, we measured the *in vitro* and *in vivo* potency of  $Mn^{2+}$  to extinguish the fura-2 fluorescence (see Methods) so that the intracellular  $[Mn^{2+}]$  that should be reached and, consequently, the  $Mn^{2+}$  current that should flow through the sarcolemma could be estimated. The  $Mn^{2+}$ -induced quenching of fura-2 fluorescence obtained in glass tubes is shown in Fig. 4A (open symbols). Fitting the relationship between the mean relative change in fura-2 fluorescence and the  $[Mn^{2+}]$  with a Hill equation gave values of  $K_{0.5}$  and  $N$  of 24  $\mu$ M and 1. The  $Mn^{2+}$ -induced quenching of fura-2 fluorescence was also measured *in vivo* by exposing fibers to various  $[Mn^{2+}]$  in the presence of the  $Ca^{2+}$  ionophore ionomycin (Fig. 4B). Fitting the relationship between the mean relative change in fura-2 fluorescence and the  $[Mn^{2+}]$  with a Hill equation gave values of  $K_{0.5}$  and  $N$  of 9.6  $\mu$ M and 0.7 (Fig. 4A, closed symbols). The main difference compared to glass tubes was that fura-2 fluorescence within the cells never dropped below 20 % of the initial fluorescence even in the presence of millimolar  $Mn^{2+}$  suggesting that part of the dye has been trapped in cell compartments out of reach of  $Mn^{2+}$ . Using the *in vivo* relationship and the measured membrane surface area in each cell tested (see Methods), the quenching rates measured at different membrane potentials were converted into membrane current densities (Fig. 4C). At -80 mV the calculated average current density was  $2.2 \pm 0.6$  mA/F and the amplitude of the membrane current in the 10 cells tested at -80 mV ranged from 0.8 to 9.8 pA, values which are far below the resolution capacity under voltage clamp conditions in the whole cell configuration.

### **$Mn^{2+}$ entry in active muscle**

Another series of experiments was carried out in order to explore whether  $Mn^{2+}$  entry could be modified by muscle activity. Trains of AP were evoked at tetanic frequency (50 Hz) under current clamp conditions in cells loaded with fura-2 and the rate of decrease of fluorescence induced by the  $Mn^{2+}$  entry was simultaneously monitored (Fig. 5A). The fluorescence intensity was not changed in response to fiber stimulation in the absence of external  $Mn^{2+}$  giving evidence that basal resting fluorescence was not altered by intracellular  $Ca^{2+}$  changes in fibers excited at 360 nm. Then, during the continuous presence of  $Mn^{2+}$ , two consecutive bursts of AP induced a large increase in the influx of  $Mn^{2+}$ . The  $Mn^{2+}$  influx was on average  $29 \pm 4$  times higher ( $n = 18$ ,  $P < 0.001$ , paired  $t$ -test) during a train of AP than under resting conditions.

Previous studies performed on adult skeletal muscle cells have shown that  $Mn^{2+}$  entry can be increased by depolarization (13) and by depletion of the SR (10) which possibly occurs during

activity. A first set of experiments aimed at exploring how store depletion could alter  $Mn^{2+}$  quenching. As illustrated in Fig. 5A, trains of AP first induced an increase in the influx of  $Mn^{2+}$  (Fig. 5B). After returning to resting conditions, addition of the potent inhibitor of the SR  $Ca^{2+}$ -ATPase CPA to the external solution did not induce any major change in the rate of  $Mn^{2+}$  influx in this cell although in average the drug evoked a slight but significant decrease of  $23 \pm 8$  % in the quenching rate ( $n = 14$ ,  $P = 0.014$ , paired  $t$ -test). In the continuous presence of CPA, a train of stimulations evoked an elevation of fura-2 fluorescence which likely resulted from the prolonged contracture of the cell that concentrated the dye. Upon repolarization, the resting influx of  $Mn^{2+}$  was increased and in average it was  $1.8 \pm 0.4$  times ( $n = 11$ ,  $P = 0.045$ , paired  $t$ -test) that measured before stimulation. Also, measurement of the voltage drop resulting from hyperpolarizing pulses of 2 nA amplitude indicated that the input resistance of the cell was not significantly changed in the presence of CPA after ( $5.4 \pm 0.5$  M $\Omega$ ) as compared to before stimulation ( $5.5 \pm 0.5$  M $\Omega$ ) ( $n = 11$ ,  $P = 0.11$ , paired  $t$ -test). The resting membrane potential was also not significantly changed ( $-83.1 \pm 0.38$  mV before and  $-82.6 \pm 0.64$  after stimulation,  $n = 11$ ,  $P = 0.29$ , paired  $t$ -test). SR depletion was certainly only partial under our experimental conditions because fibers still contracted in the presence of CPA although they contracted weaker and failed to relax after stimulation. However, all our attempts to induce more severe depletion to the point of complete fiber exhaustion systematically led to an irreversible depolarization of the fiber associated with a large fall in the input resistance and a profound and irreversible increase in the influx of  $Mn^{2+}$  that saturated the dye. Figure 5C illustrates such behaviour in a particular fiber which displayed irreversible damages as soon as stimulation was delivered in the presence of CPA. This result emphasizes that voltage control is essential to monitor cell integrity during quenching experiments.

### **Voltage dependence and $Cd^{2+}$ inhibition of $Mn^{2+}$ influx in active muscle**

Another set of experiments was carried out to investigate how depolarization by itself initiates  $Mn^{2+}$  influx.  $Mn^{2+}$  influx together with membrane currents were measured in fibers stimulated by voltage pulses of increasing amplitudes in the presence of 3 mM  $Mn^{2+}$ . In these experiments, the possible contribution of a store-operated  $Mn^{2+}$  influx should be largely minimized since depolarization has been demonstrated to strongly inhibit store-operated  $Mn^{2+}$  influx (10). Figure 6 shows that 100 ms duration depolarizing pulses given to -50, -30 and -10 mV did not change the rate of  $Mn^{2+}$  influx. A pulse to +10 mV induced an inward  $Mn^{2+}$  current which reached -1.9 nA, associated with a 9.2 % decrease in fluorescence. A subsequent pulse to +30 mV gave rise to an inward  $Mn^{2+}$  current which activated faster and reached -2.1 nA, accompanied by a 14.6 % drop in fluorescence. Finally, a last pulse to +50 mV induced an outward membrane current associated with a 12 % decrease in fluorescence. Inward currents evoked by membrane depolarization were completely blocked by the addition of 0.5 mM  $Cd^{2+}$  in the external solution (Fig. 7A). Taken together, these data likely indicated that the recorded  $Mn^{2+}$  current flowed through L-type  $Ca^{2+}$  channels which are known to be permeable to  $Mn^{2+}$  in skeletal muscle (18). Figure 7A presents the voltage-current relationship of the  $Mn^{2+}$  current and Figure 7B superimposes the relationship between the magnitude of the fluorescence decrease induced by  $Mn^{2+}$  entry and voltage and the voltage dependence of the relative conductance of the  $Mn^{2+}$  current. It can be observed that the voltage-activated  $Mn^{2+}$  current and the  $Mn^{2+}$  influx were maximal around +30 mV. Fitting Boltzmann equations to these two relationships indicated that  $V_{0.5}$  was 24 mV more negative for the  $Mn^{2+}$  influx than for the voltage-activated current and that the voltage dependence of the  $Mn^{2+}$  influx was steeper than the one of the normalized conductance ( $k$  was 4.7 as compared to 8.6) (Fig. 7B). Differences suggest that at least two processes displaying dissimilar voltage dependences may contribute to the influx of  $Mn^{2+}$ : the L-type current and a parallel voltage-activated  $Mn^{2+}$

entry. In order to determine to what extent each of these two processes contributed to the influx of divalent cations during physiological activation of muscle cells, the effects of a blockade of the L-type current by  $\text{Cd}^{2+}$  were tested on the influx of  $\text{Mn}^{2+}$  induced by trains of AP. As illustrated in Fig. 8C, the mean drop in fluorescence induced by the train of excitation in the presence of  $\text{Cd}^{2+}$  (0.5 mM) was not significantly different from the one induced in its absence ( $n = 9$ ,  $P = 0.39$ , paired  $t$ -test). This result can be interpreted in two ways. Either the L-type current is not activated during trains of AP, or the L-type current is activated, but the influx of  $\text{Mn}^{2+}$  that this current generates does not contribute significantly to the quenching of fluorescence induced by depolarization. In order to discriminate between these two possibilities, we tested the effects of  $\text{Cd}^{2+}$  on the  $\text{Mn}^{2+}$  influx induced by depolarization. Figure 7D shows that the decrease in fluorescence in response to a depolarization to +30 mV that evoked an L-type current of maximal amplitude was greatly reduced in the presence of  $\text{Cd}^{2+}$ . Figure 7B presents the mean changes in fluorescence induced by different depolarization pulses in the presence of  $\text{Cd}^{2+}$ . On average, the  $\text{Mn}^{2+}$  influx was significantly reduced by 72, 76 and 82 % for depolarization steps to +10, +30 and +50 mV in the presence of  $\text{Cd}^{2+}$  but was not significantly affected for pulses to -10 mV ( $P = 0.46$ , unpaired  $t$ -test) (Fig. 7B). Figure 7B also indicated that a substantial  $\text{Mn}^{2+}$  influx occurred through L-type channels at the reversal potential of the L-type current; however this reversal potential value was likely shifted toward negative voltages by contaminating outward currents so that there still was a driving force for  $\text{Mn}^{2+}$  influx at +50 mV. Fitting a Boltzmann equation to the relationship between mean changes of fluorescence and membrane potential in the presence of  $\text{Cd}^{2+}$  gave value for  $V_{0.5}$  and  $k$  of -8 mV and 4 mV.

## Discussion

### Properties of divalent cation influx at rest and associated membrane current

In the first part of the present study, the combination of the  $\text{Mn}^{2+}$  quenching method with a voltage clamp technique together with calibration of the fura-2 response to  $\text{Mn}^{2+}$  allowed us to thoroughly characterize the influx of divalent cations at rest in isolated adult skeletal muscle fibers. At a holding potential of -80 mV and in the presence of 500  $\mu\text{M}$  external  $\text{Mn}^{2+}$ , the rate of  $\text{Mn}^{2+}$  influx was found to be 4.5 %. $\text{min}^{-1}$  in average, a value close to the values reported in other studies using the same external  $[\text{Mn}^{2+}]$  on adult mouse muscle fibers at rest (5, 9, 10, 19). The rate of quenching was found to depend on the  $\text{Mn}^{2+}$  concentration and on the electrical gradient. The voltage dependence of the rate of quenching indicated that the influx of  $\text{Mn}^{2+}$  was slightly favoured at negative membrane potentials, a result which explains that hyperpolarizing steps were less effective in increasing the quenching rate when they were applied from depolarized holding potentials. This apparent inward rectification may either result from intrinsic properties of the pathway involved or may be due to the fact that a  $\text{Mn}^{2+}$  equilibrium potential can never be reached because  $\text{Mn}^{2+}$  ions are supposed to be unable to move out of the cell. Finally, we observed that the quenching rate was reduced by more than half when  $\text{Ca}^{2+}$  ions were present at physiological concentrations in the external solution, which indicates that  $\text{Ca}^{2+}$  compete with  $\text{Mn}^{2+}$  for permeating the influx pathway.

The combined use of voltage clamp and  $\text{Mn}^{2+}$  quenching techniques prompted us to try measuring the inward current which may be associated with  $\text{Mn}^{2+}$  entry.  $\text{Mn}^{2+}$  exerted a strong blocking effect on muscle background conductances which precludes revealing a putative inward current upon replacement of  $\text{Mg}^{2+}$  by  $\text{Mn}^{2+}$ . Nevertheless, our *in vivo* calibration experiments of the fura-2 response to  $\text{Mn}^{2+}$  predicted that the inward current generated by the influx of  $\text{Mn}^{2+}$  should have had amplitudes of a few picoamps in the presence of millimolar external  $[\text{Mn}^{2+}]$  which are clearly undetectable at the macroscopic level. At first sight, these results are hardly reconcilable with data obtained at the single

channel level. Openings of spontaneously active  $\text{Ca}^{2+}$  channels are indeed routinely recorded in cell-attached patches at negative voltages (6) and these channels were found to be permeant to  $\text{Mn}^{2+}$  (5). However, no correlation was found between subsarcolemmal  $\text{Ca}^{2+}$  load and activity of these channels suggesting that they are not involved in resting  $\text{Ca}^{2+}$  influx (7). For obscure reasons, a parallel pathway which does not produce resolvable current could thus be more efficient in getting  $\text{Ca}^{2+}$  in. Yet, the fact that  $\text{Mn}^{2+}$  entry is driven by the concentration and electrical gradients strongly suggests that  $\text{Mn}^{2+}$  and  $\text{Ca}^{2+}$  enter muscle cells through ion channels spontaneously open at rest and necessarily of very low conductance. However, the involvement of electrically silent transport processes directly or indirectly influenced by the concentration and electrical gradients cannot be excluded and deserves further attention. Finally our study demonstrates that, because  $\text{Mn}^{2+}$  accumulates in the cytosol, the  $\text{Mn}^{2+}$  quenching method offers a higher resolution to monitor the entry of divalent cations at rest than the measurement of currents.

### **Store depletion-activated cation influx**

We demonstrated here that a single burst of AP delivered in the presence of CPA significantly increased the resting rate of  $\text{Mn}^{2+}$  influx. We observed that fibers still contracted in response to stimulation in the presence of CPA, indicating that store depletion was not complete under our experimental conditions. In our hands, attempts to provoke deeper depletion of the SR inevitably led to a huge influx of  $\text{Mn}^{2+}$  and an irreversible depolarization of the fiber associated with a large decrease in the input resistance which gave evidence of irreversible damages of the sarcolemma, possibly produced by toxic elevation of the intracellular  $[\text{Ca}^{2+}]$ . As pointed out by Kurebayashi & Ogawa (10), severe  $\text{Ca}^{2+}$  depletion to the point of complete exhaustion of contraction would certainly never occur in adult skeletal muscle under physiological conditions. Our experiments show that partial depletion does induce  $\text{Ca}^{2+}$  entry as described by Launikonis & Rios (20) in skinned rat muscle fibers. Confirming our previous data (12), these experiments also demonstrate that the store-operated  $\text{Ca}^{2+}$  entry was not associated with the development of a measurable current as evidenced by the absence of a significant change in the cell input resistance and membrane potential. This series of experiments also indicates that experiments making use of SR  $\text{Ca}^{2+}$ -ATPase inhibitors have to be interpreted with caution when they are performed in the absence of voltage control. Background current or membrane potential and input resistance measurement are very reliable indexes of cell integrity that may reveal massive damages of the sarcolemma not related to any store-operated pathway.

### **Cation influx activated by trains of AP**

We found that trains of AP delivered at 50 Hz, which closely correspond to physiological conditions of stimulation, increased  $\text{Mn}^{2+}$  influx to a much greater degree (29 fold in the presence of 3 mM external  $\text{Mn}^{2+}$ ) as compared to store depletion. The control of the membrane potential allowed us to explore the  $\text{Mn}^{2+}$  influx over a large range of membrane voltages. The following observations led us to conclude that the L-type voltage-activated  $\text{Ca}^{2+}$  channels and a parallel distinct voltage-activated  $\text{Mn}^{2+}$  pathway contributed independently to the  $\text{Mn}^{2+}$  influx in response to depolarization: (i) the voltage dependence of the global  $\text{Mn}^{2+}$  influx was steeper than the one of the L-type  $\text{Mn}^{2+}$  current and shifted toward negative potentials; (ii) whereas  $\text{Cd}^{2+}$  entirely inhibited the L-type  $\text{Mn}^{2+}$  current, a  $\text{Mn}^{2+}$  influx still occurred in response to depolarization with a voltage threshold and voltage dependence that were respectively lower and steeper than those of the L-type current. Our  $\text{Cd}^{2+}$  experiments also allowed us to estimate the relative contribution of each of these divalent cations entries during muscle activation at different voltages. At -10 mV, the newly identified voltage-activated  $\text{Mn}^{2+}$  influx pathway may contribute mainly to the global  $\text{Mn}^{2+}$  influx while for

higher depolarizations it may represent between 18 and 28 % of the total  $Mn^{2+}$  influx. A striking observation was that no net inward current persisted when the L-type current was inhibited by  $Cd^{2+}$ . Yet, if this influx represents 24 % of the global entry at +30 mV, we should have been able to record a net inward current after  $Cd^{2+}$  blockade whose amplitude should also represent one quarter of the amplitude of the L-type current. A similar phenomenon identified as excitation-coupled  $Ca^{2+}$  entry has been described in myotubes (13) and, interestingly, current recordings on myotubes expressing a mutant isoform of type 1 ryanodine receptor also failed to reveal a current associated with this  $Mn^{2+}$  entry although the magnitude of the  $Ca^{2+}$  entry produced predicted that a current larger than the L-type current should have developed (21). As postulated for myotubes, our results suggest that a voltage-activated  $Mn^{2+}$  influx operates in an electrically silent manner in adult skeletal muscle. One possibility is that this  $Mn^{2+}$  influx involves a non electrogenic exchanger, which up to now has never been described, but actually merits further consideration.

### **Physiological significance of activity-induced cation influx**

A more striking result was that  $Cd^{2+}$  did not affect the  $Mn^{2+}$  influx induced by train of AP. Apart from the fact that this result confirms that a voltage-activated  $Mn^{2+}$  influx insensitive to  $Cd^{2+}$  does operate in adult skeletal muscle in parallel with the L-type current, these data also suggest that the L-type current does not contribute to the influx of divalent cations during physiological excitation. However, this last result must be taken with caution because the voltage dependence of the  $Mn^{2+}$  current through L-type channels was shifted by 23 mV toward positive membrane potentials ( $V_{0.5} = +22$  mV) as compared to the voltage dependence of the  $Ca^{2+}$  current in the presence of 2.5 mM external  $Ca^{2+}$  ( $V_{0.5} = -0.7$  mV in 22). The membrane potential reached in response to trains of AP could thus be far above the peak value of the L-type  $Ca^{2+}$  current but lower than the one of the  $Mn^{2+}$  current so that the contribution of the L-type current may be minimized when  $Mn^{2+}$  ions are flowing through the channels. Whatever the pathway involved, the physiological role of the  $Ca^{2+}$  influx during excitation remains largely elusive in skeletal muscle. A current hypothesis suggests that the  $Ca^{2+}$  entry induced by depolarization or by SR depletion may contribute to refill internal  $Ca^{2+}$  stores especially under fatigue conditions. However, it was shown that the recovery of the releasable pool after fatigue occurred in the absence of extracellular  $Ca^{2+}$  (23) and growing evidences indicate that  $Ca^{2+}$  is not extruded from the cells during fatigue but may remain as a non releasable pool possibly bound to phosphate within the SR (24). Within this context, we believe that the nature and the physiological role of the  $Ca^{2+}$  pathways involved during excitation still remain open questions in adult skeletal muscle which call for further attention.

### **Acknowledgements**

This work was supported by the Université Lyon 1, the Centre National de la Recherche Scientifique, the Association Française contre les Myopathies and the Agence Nationale de la Recherche Maladies Rares. We are grateful to J-L. Barrat, M. Jospin and V. Jacquemond for helpful comments on the manuscript.

### **References**

1. Clausen, T., A. B. Dahl-Hansen, and J. Elbrink. 1979. The effect of hyperosmolarity and insulin on resting tension and calcium fluxes in rat soleus muscle. *J. Physiol.* 292:505-526.
2. Gailly, P. 2002. New aspects of calcium signaling in skeletal muscle cells: implications in Duchenne muscular dystrophy. *Biochim. Biophys. Acta* 1600:38-44.

3. Haws, C. M., and J. B. Lansman. 1991. Developmental regulation of mechanosensitive calcium channels in skeletal muscle from normal and *mdx* mice. *Proc. Biol. Sci.* 245:173-177.
4. Hopf, F. W., P. R. Turner, W. F. Denetclaw Jr, P. Reddy, and R. A. Steinhardt. 1996. A critical evaluation of resting intracellular free calcium regulation in dystrophic *mdx* muscle. *Am. J. Physiol.* 271:C1325-1339.
5. De Backer, F., C. Vandebrouck, P. Gailly, and J. M. Gillis. 2002. Long-term study of Ca<sup>2+</sup> homeostasis and of survival in collagenase-isolated muscle fibres from normal and *mdx* mice. *J. Physiol.* 542:855-865.
6. Allard, B. 2006. Sarcolemmal ion channels in dystrophin-deficient skeletal muscle fibres. *J. Muscle Res. Cell Motil.* 27:367-373.
7. Mallouk, N., and B. Allard. 2002. Ca<sup>2+</sup> influx and opening of Ca<sup>2+</sup>-activated K<sup>+</sup> channels in muscle fibers from control and *mdx* mice. *Biophys. J.* 82:3012-3021.
8. Merritt, J. E., R. Jacob, and T. J. Hallam. 1989. Use of manganese to discriminate between calcium influx and mobilization from internal stores in stimulated human neutrophils. *J. Biol. Chem.* 264:1522-1527.
9. Tutdibi, O., H. Brinkmeier, R. Rüdell, and K. J. Föhr. 1999. Increased calcium entry into dystrophin-deficient muscle fibres of MDX and ADR-MDX mice is reduced by ion channel blockers. *J. Physiol.* 515:859-868.
10. Kurebayashi, N., and Ogawa, Y. 2001. Depletion of Ca<sup>2+</sup> in the sarcoplasmic reticulum stimulates Ca<sup>2+</sup> entry into mouse skeletal muscle fibres. *J. Physiol.* 533:185-199.
11. Collet, C., and J. Ma. 2004. Calcium-dependent facilitation and graded deactivation of store-operated calcium entry in fetal skeletal muscle. *Biophys. J.* 87:268-275.
12. Allard, B., H. Couchoux, S. Pouvreau, and V. Jacquemond. 2006. Sarcoplasmic reticulum Ca<sup>2+</sup> release and depletion fail to affect sarcolemmal ion channel activity in mouse skeletal muscle. *J. Physiol.* 575:69-81.
13. Cherednichenko, G., A. M. Hurne, J. D. Fessenden, E. H. Lee, P. D. Allen, K. G. Beam, and I. N. Pessah. 2004. Conformational activation of Ca<sup>2+</sup> entry by depolarization of skeletal myotubes. *Proc. Natl. Acad. Sci. USA.* 101:15793-15798.
14. Cherednichenko, G., C. W. Ward, W. Feng, E. Cabrales, L. Michaelson, M. Samsó, J. R. López, P. D. Allen, and I. N. Pessah. 2008. Enhanced excitation-coupled calcium entry in myotubes expressing malignant hyperthermia mutation R163C is attenuated by dantrolene. *Mol. Pharmacol.* 73:1203-1212.
15. Jacquemond, V., and B. Allard. 1998. Activation of Ca<sup>2+</sup>-activated K<sup>+</sup> channels by an increase in intracellular Ca<sup>2+</sup> induced by depolarization of mouse skeletal muscle fibres. *J. Physiol.* 509:93-102.
16. Weiss, N., H. Couchoux, C. Legrand, C. Berthier, B. Allard, and V. Jacquemond. 2008. Expression of the muscular dystrophy-associated caveolin-3<sup>P104L</sup> mutant in adult mouse skeletal muscle specifically alters the Ca<sup>2+</sup> channel function of the dihydropyridine receptor. *Pflugers Arch.* In press.
17. Jacquemond, V. 1997. Indo-1 fluorescence signals elicited by membrane depolarization in enzymatically isolated mouse skeletal muscle fibers. *Biophys. J.* 73:920-928.
18. Almers, W., and P. T. Palade. 1981. Slow calcium and potassium currents across frog muscle membrane: measurements with a vaseline-gap technique. *J. Physiol.* 312:159-176.
19. Fraysse, B., J. F. Desaphy, S. Pierno, A. De Luca, A. Liantonio, C. I. Mitolo, and D. C. Camerino. 2003. Decrease in resting calcium and calcium entry associated with slow-to-fast transition in unloaded rat soleus muscle. *FASEB J.* 17:1916-1918.
20. Launikonis, B. S., and E. Ríos. 2007. Store-operated Ca<sup>2+</sup> entry during intracellular Ca<sup>2+</sup> release in mammalian skeletal muscle. *J. Physiol.* 583:81-97.
21. Hurne, A. M., J. J. O'Brien, D. Wingrove, G. Cherednichenko, P. D. Allen, K. G. Beam, and I. N. Pessah. 2005. Ryanodine receptor type 1 (RyR1) mutations C4958S and C4961S

reveal excitation-coupled calcium entry (ECCE) is independent of sarcoplasmic reticulum store depletion. *J. Biol. Chem.* 280:36994-37004.

22. Collet, C., L. Csernoch, and V. Jacquemond. 2003. Intramembrane charge movement and L-type calcium current in skeletal muscle fibers isolated from control and *mdx* mice. *Biophys. J.* 84:251-265.

23. Kabbara, A. A., and D. G. Allen. 1999. The role of calcium stores in fatigue of isolated single muscle fibres from the cane toad. *J. Physiol.* 519:169-176.

24. Allen, D. G., G. D. Lamb, and H. Westerblad. 2008. Skeletal muscle fatigue: cellular mechanisms. *Physiol. Rev.* 88:287-332.

## Figure legends

**Figure 1: Influence of the external  $Mn^{2+}$  concentration on  $Mn^{2+}$  influx at -80 mV.** The bars indicate the periods during which the cell was exposed to an external Tyrode solution containing 3 mM  $Mn^{2+}$  (A) and 1 mM or 10 mM  $Mn^{2+}$  (B). The straight lines superimposed correspond to the linear regressions fitted to the fluorescence records with slopes of 27 %/min in A and 14 and 38 %/min in B. (C) The histogram shows the average values of quenching rate obtained in the presence of increasing external  $Mn^{2+}$  concentrations. The numbers above each bar indicate the number of cells tested.

**Figure 2: Influence of membrane potential on  $Mn^{2+}$  influx in the presence of 3 mM external  $Mn^{2+}$ .** (A) Effect of addition of  $Mn^{2+}$  on fura-2 fluorescence at the indicated voltages in four different cells. The slopes of the linear fits are 8, 13, 20 and 29 %/min at +40, 0, -40 and -80 mV respectively. (B) Average values of quenching rate obtained at different membrane voltages. (C) Changes in the quenching rate induced by a 60mV-hyperpolarizing pulse given from a holding potential of +20 mV (upper trace) and -20 mV (lower trace). The slope of the linear fits increased from 9 to 13 %/min in the upper trace and from 15 to 29 %/min in the lower trace. (D) Effect of the holding potential on the change in the quenching rate induced by a 60mV-hyperpolarizing pulse.

**Figure 3: Membrane currents evoked by replacement of  $Mg^{2+}$  by  $Mn^{2+}$ .** (A and B) Simultaneous recordings of membrane currents and fura-2 fluorescence at -80 mV and +40 mV. The slope of the linear fit is 24 and 12 %/min at -80 and +40 mV respectively. (C) Continuous recording of membrane current at -80 mV in response to replacement of 10 mM  $Mg^{2+}$  by 10 mM  $Mn^{2+}$ . The cell was challenged by voltage ramps given from -40 to -100 mV at a rate of 120mV/s every 5 s in the presence of 140 mM external TEA-methanesulfonate plus 9AC and 120 mM internal Cs-aspartate. (D) Current-voltage relationships obtained in the fiber illustrated in (C) in response to voltage ramps, the lower and upper traces corresponding to the left and right arrows in (C) respectively.

**Figure 4: Estimation of the sarcolemmal  $Mn^{2+}$  current on the basis of the measurement of the changes in fura-2 fluorescence induced by  $Mn^{2+}$  entry.** (A) Relationships between the relative fluorescence of fura-2 and the concentration of  $Mn^{2+}$  in glass tubes (open symbols,  $n = 9$ ), and the concentration of  $Mn^{2+}$  in the external solution bathing muscle fibers in the presence of ionomycin (closed symbols,  $n = 4$ ). Curves were fitted using a Hill equation (see text for details). (B) Quenching of fura-2 fluorescence obtained in a fiber exposed to the indicated concentrations of  $Mn^{2+}$  in the presence of ionomycin. (C) Relationship between the estimated resting  $Mn^{2+}$  current and membrane voltage. The curve was drawn by eye.

**Figure 5: Effects of trains of AP and CPA on  $Mn^{2+}$  influx under current clamp conditions.** (A) Simultaneous recordings of fura-2 fluorescence (open symbols) and membrane potential (lower trace) in a fiber stimulated by positive suprathreshold current pulses of 0.5 ms duration delivered at 50 Hz. The duration of the trains was 2 s in the left panel and 3 s in the right panel. Each burst of stimulation was preceded by a negative current pulse of 2 nA amplitude to measure the fiber input resistance (downward deflections of the voltage trace). The inset shows the first train of AP (star, left trace) and the first AP of this train (right trace) on an expanded scale. The recordings presented in the right panel were obtained in the same fiber 4 min after the ones presented in the left panel. The external Tyrode solution contained 2 mM  $CaCl_2$  and 2 mM  $MgCl_2$  in which 1 mM  $Mn^{2+}$  was added. (B) In the continuous presence of a Tyrode solution containing 3 mM  $Mn^{2+}$ , the fiber was stimulated by bursts of AP of 500 ms duration delivered at 50 Hz in the absence and in the presence of CPA. Fluorescence records were fitted with a linear regression in the presence of CPA with slopes of 4 %/min before and of 10 %/min after stimulation. (C) In this particular fiber, a single burst of AP given in the presence of CPA led to a brutal drop of fluorescence (the slope of the linear fit is 190 %/min) and an irreversible depolarization of the fiber. Note that membrane potential in lower traces was acquired at 200 Hz so that peak values of AP could not be resolved.

**Figure 6: Effect of depolarization steps of increasing amplitude on  $Mn^{2+}$  influx under voltage clamp conditions.** Fura-2 fluorescence (open symbols) and membrane currents (lower traces) were measured on the same muscle fiber in the presence of a 140 mM TEA-methanesulfonate  $Ca^{2+}$ -free external medium containing 3 mM  $Mn^{2+}$ . The cell was held at -80 mV and voltage steps of 100 ms duration bringing the membrane potential to the indicated values were applied between two fluorescence image captures at the indicated position of the steps. Note that the corresponding currents were positioned under the voltage steps on a different time scale.

**Figure 7: Voltage dependence of  $Mn^{2+}$  influx and effect of  $Cd^{2+}$ .** (A) The upper traces show the membrane currents recorded in a same fiber in response to a 200-ms depolarization step given to +30mV from a holding potential of -80 mV in the absence and in the presence of 0.5 mM  $Cd^{2+}$  (star) and the current-voltage relationship of the  $Mn^{2+}$  current. The curve was fitted using the equation indicated in Methods with values for  $G_{max}$ ,  $V_{rev}$ ,  $V_{0.5}$  and  $k$  of 127 S/F, +50 mV, +22 mV, and 7.9 mV ( $n = 9$ ). (B) Relationships between the mean normalized conductance of the voltage-activated  $Mn^{2+}$  current and membrane potential (closed symbols), between the mean  $Mn^{2+}$  influx, expressed as percentage of decrease of fluorescence, and membrane potential in the absence (open circles) and in the presence of 0.5 mM  $Cd^{2+}$  (open squares). The curves were fitted using a Boltzmann equation with values for  $V_{0.5}$  and  $k$  of +22 mV and 8.6 mV for the normalized conductance, -1.9 mV and 4.7 mV for the  $Mn^{2+}$  influx in the absence of  $Cd^{2+}$  and -8 mV and 4 mV for the  $Mn^{2+}$  influx in the presence of  $Cd^{2+}$ . The number of cells tested at -10, +10, +30 and +50 mV is 8, 4, 4 and 2 in the absence of  $Cd^{2+}$  and 7, 8, 8 and 1 in the presence of  $Cd^{2+}$ . (C) In the left panel, a single train of AP (lower trace) was elicited under current clamp conditions by injection of positive supraliminal current pulses of 0.5 ms duration delivered at 50 Hz in the presence of 3 mM external  $Mn^{2+}$  while fura-2 fluorescence was simultaneously recorded (open symbols). The same stimulation was applied in the same cell with 0.5 mM  $Cd^{2+}$  added in the external medium (right panel). The two consecutive recordings were separated by a 2-min interval. (D) In the left panel, the cell was held at -80 mV and a 100-ms depolarizing pulse was given to +30mV as indicated by the step at the bottom in the presence of 3 mM external  $Mn^{2+}$ . The same stimulation was applied in the same cell with 0.5 mM  $Cd^{2+}$  added in the external medium (right panel). The two

consecutive fluorescence recordings were separated by a 1-min interval. The fluorescence data points immediately before and after stimulations were linked by a straight line to make fluorescence drops more visible. The slopes of these lines were 30 and 29 %/min in the absence and in the presence of  $\text{Cd}^{2+}$  in C, respectively, and 122 and 45 %/min in D, respectively.

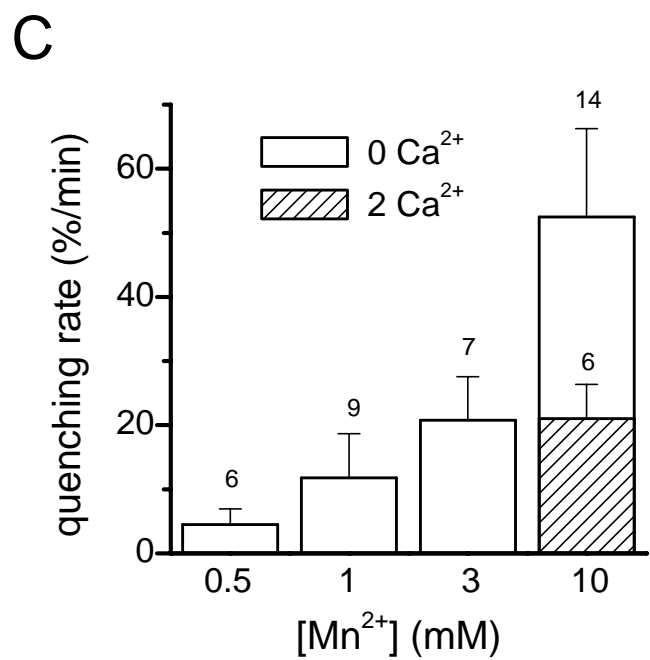
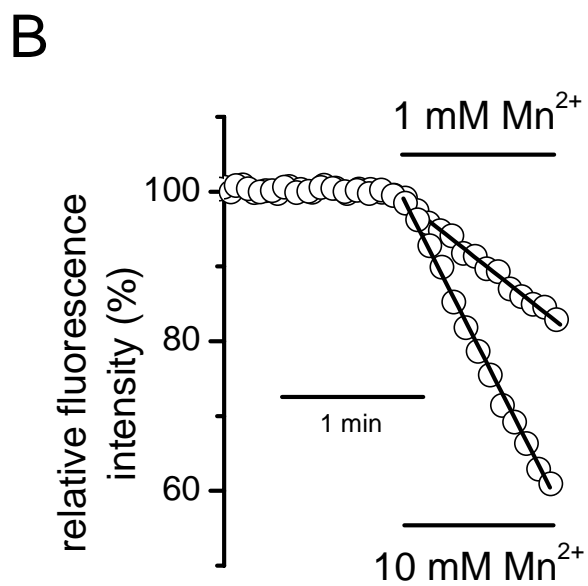
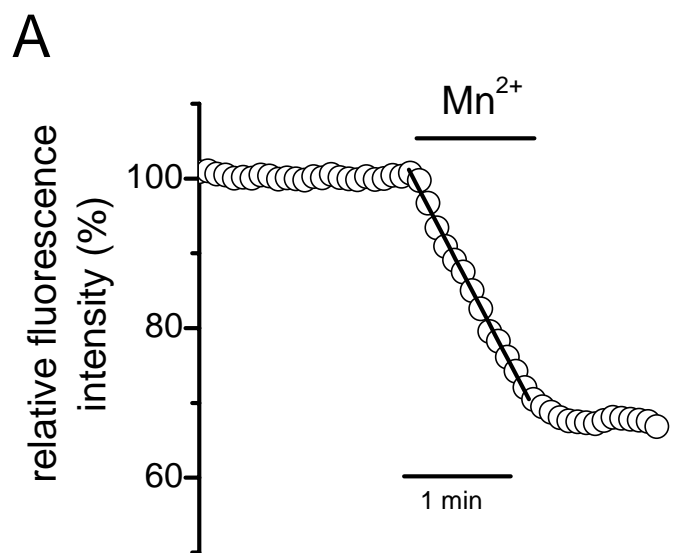


Figure 1

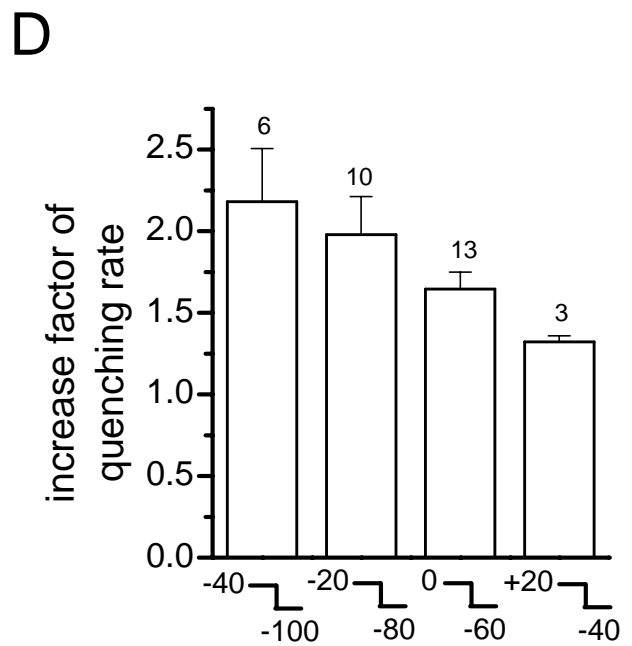
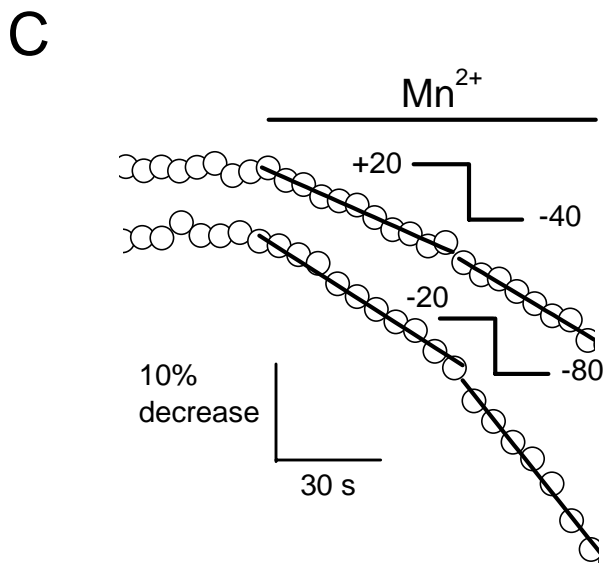
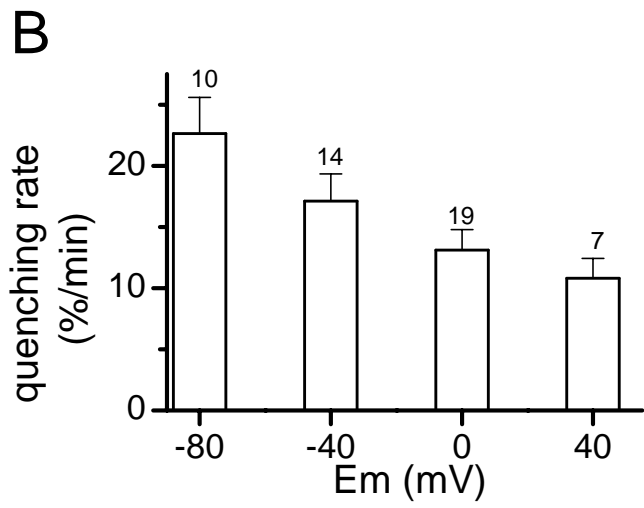
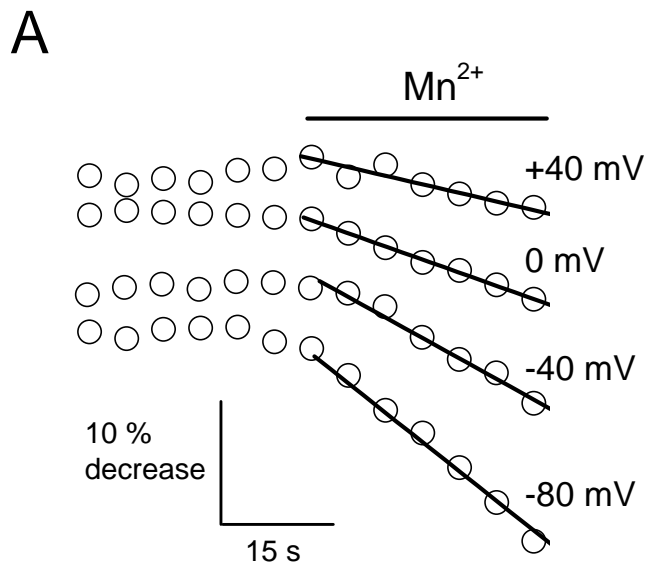


Figure 2

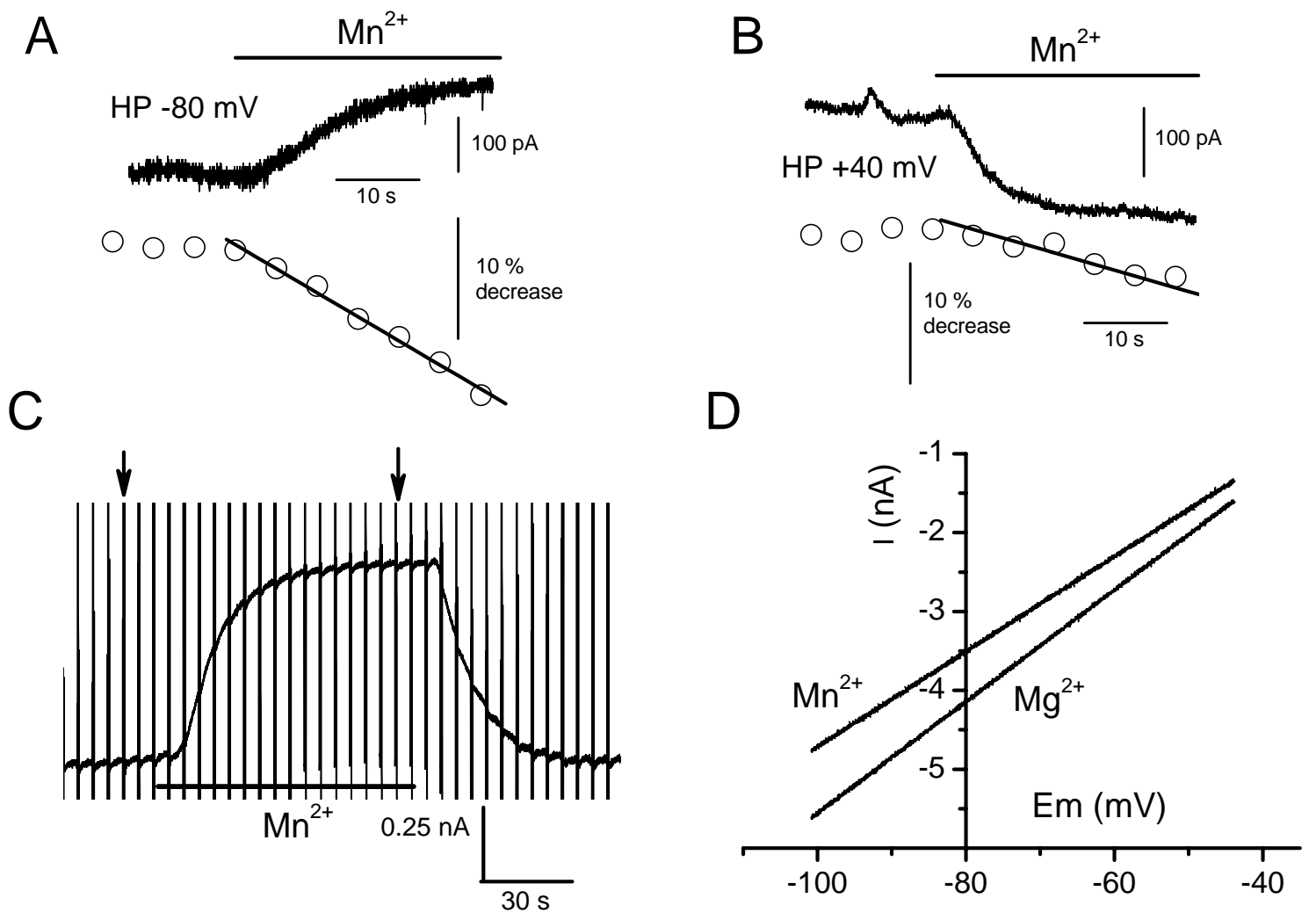


Figure 3

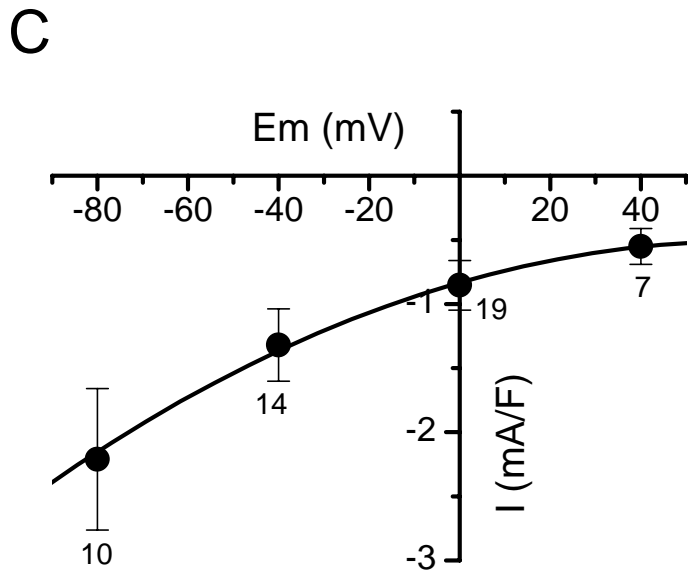
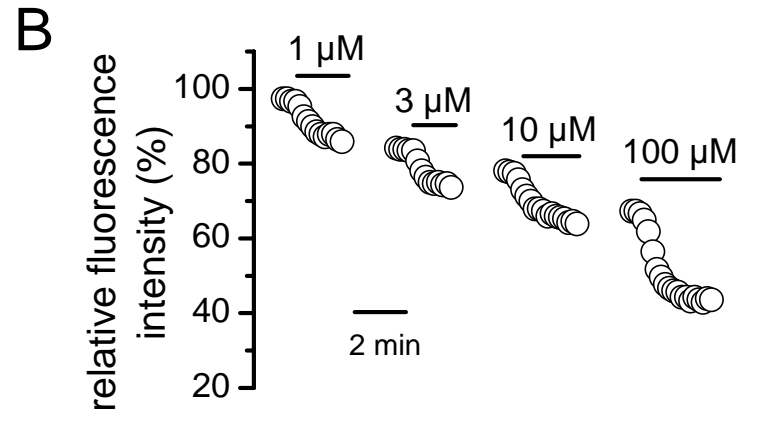
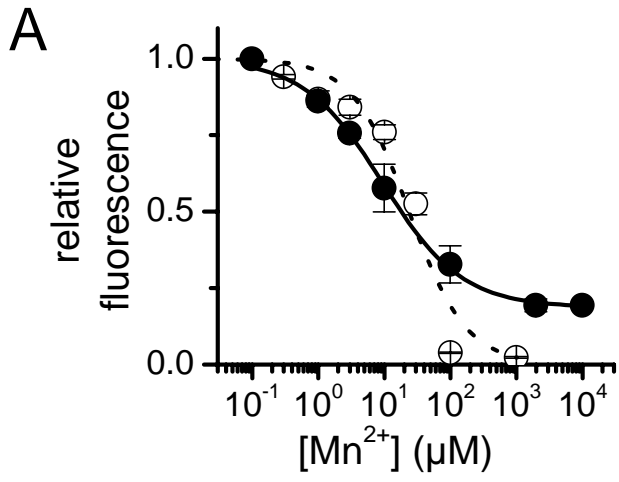


Figure 4

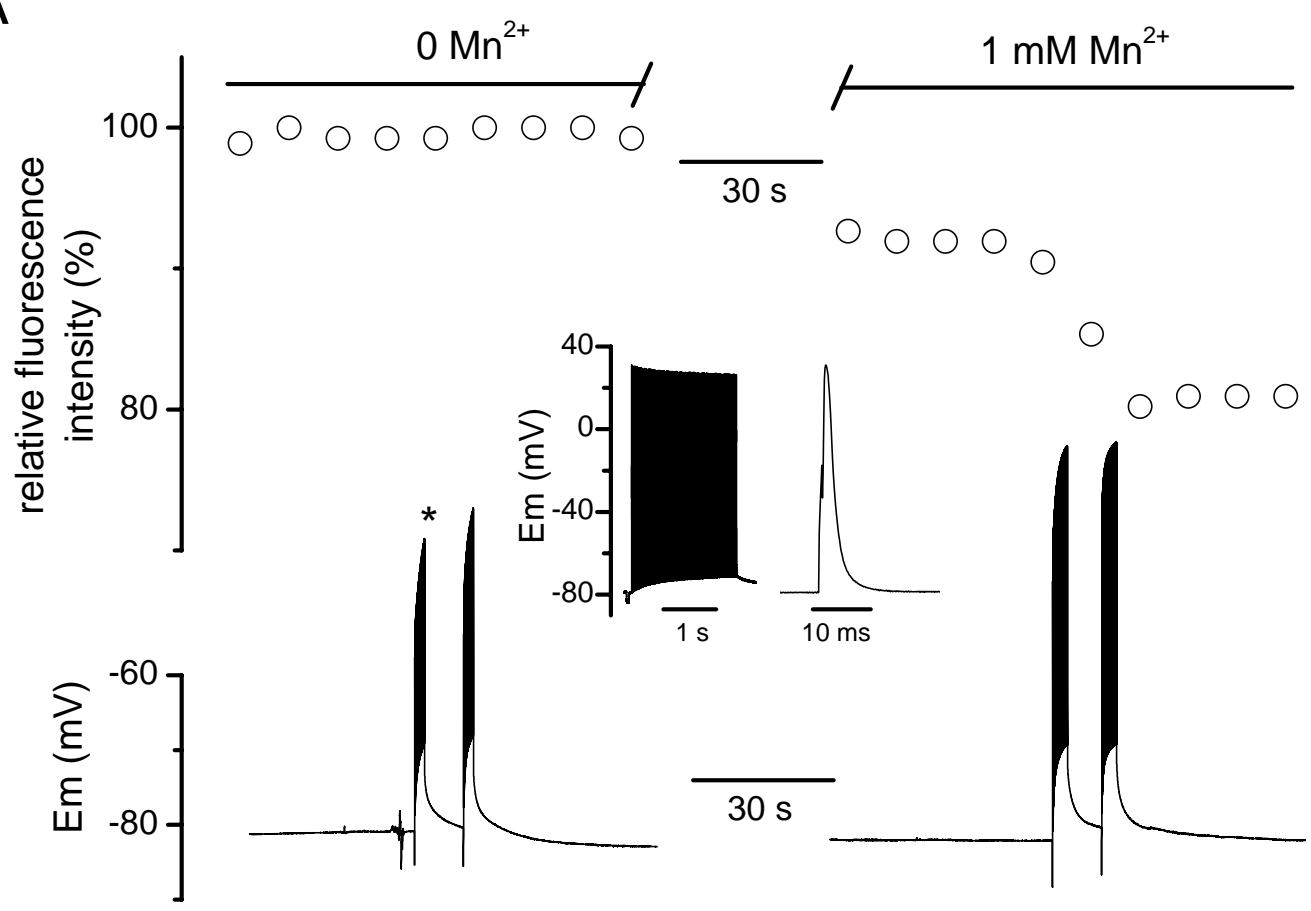
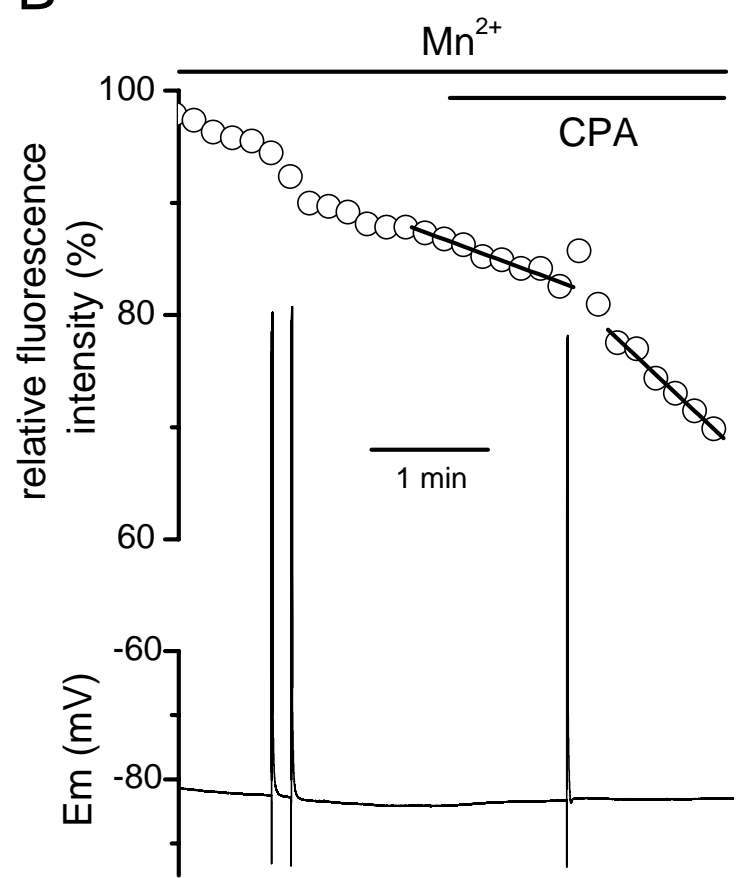
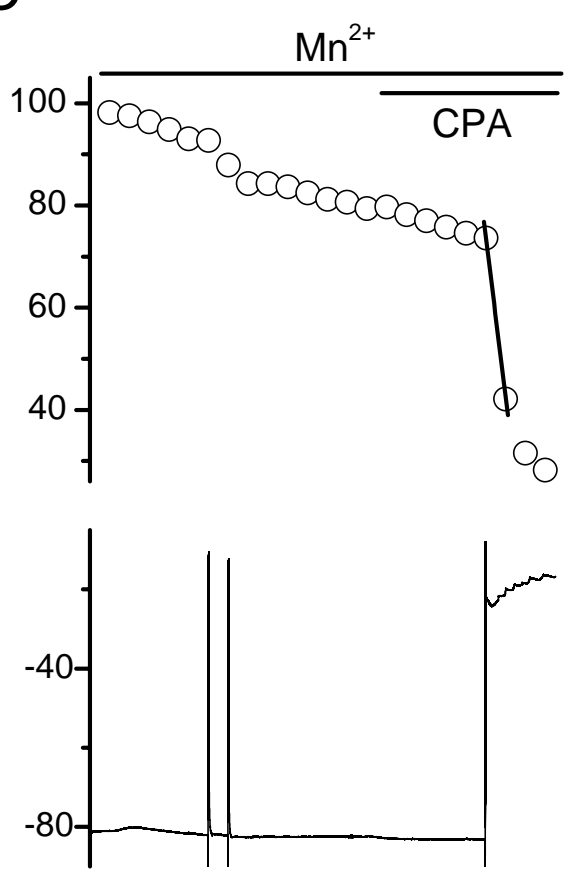
**A****B****C**

Figure 5

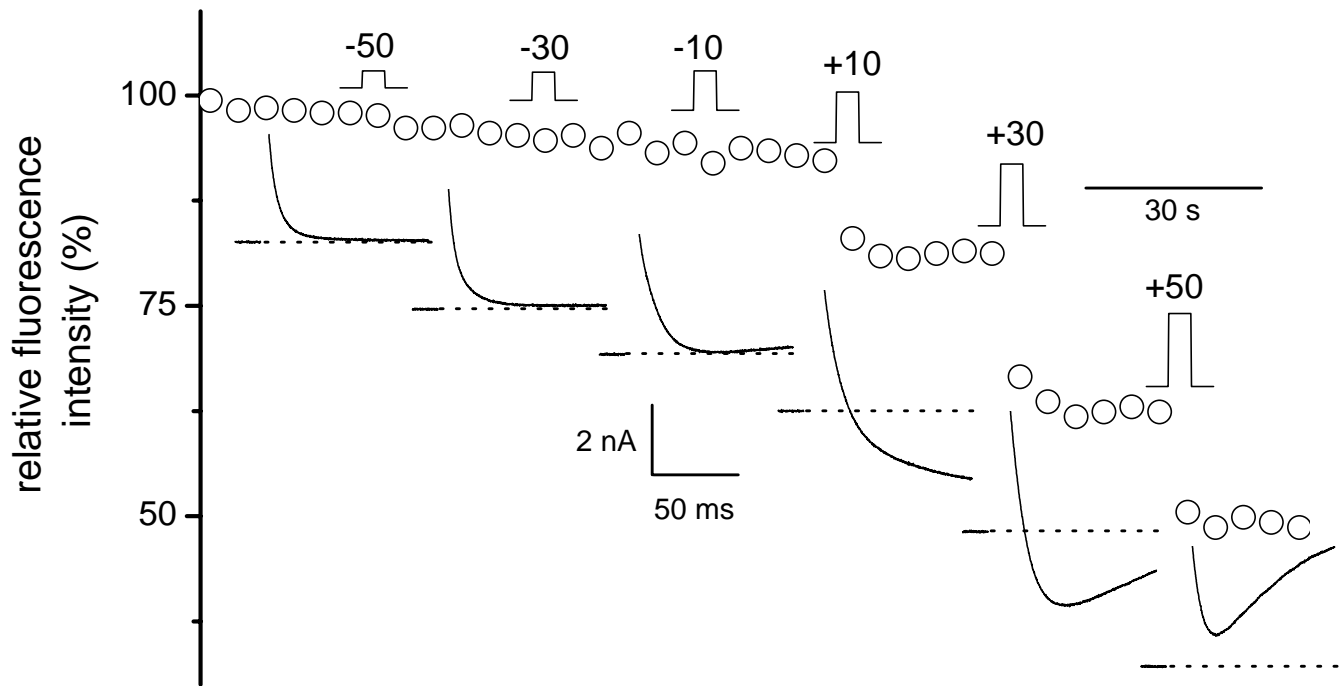


Figure 6

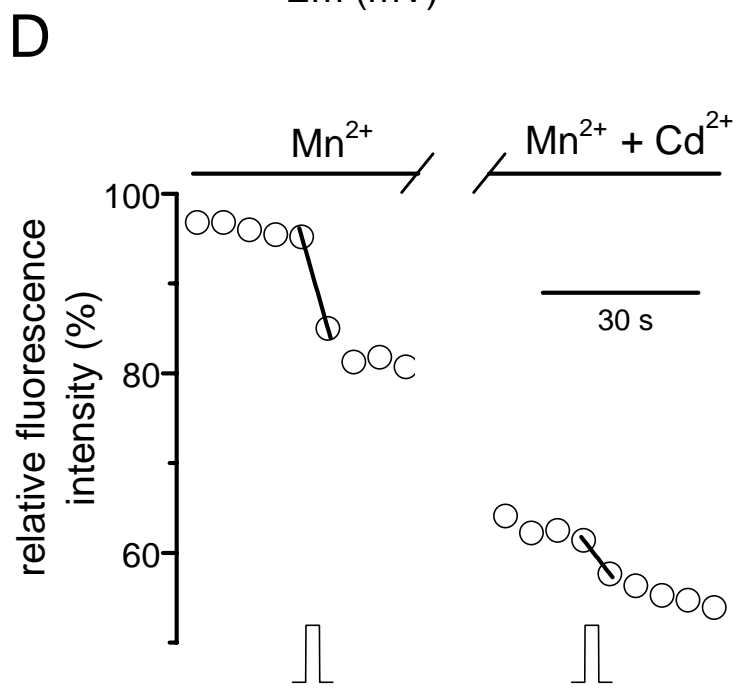
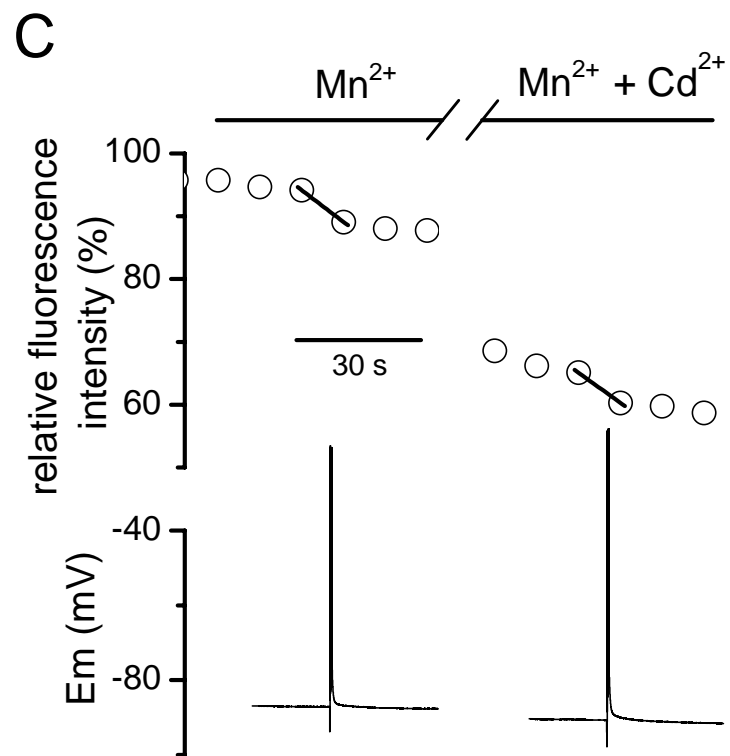
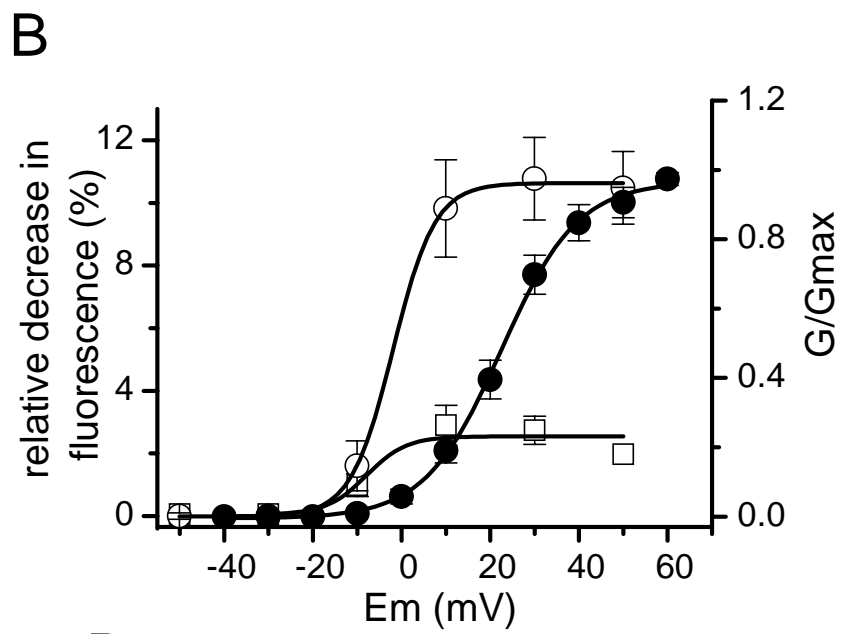
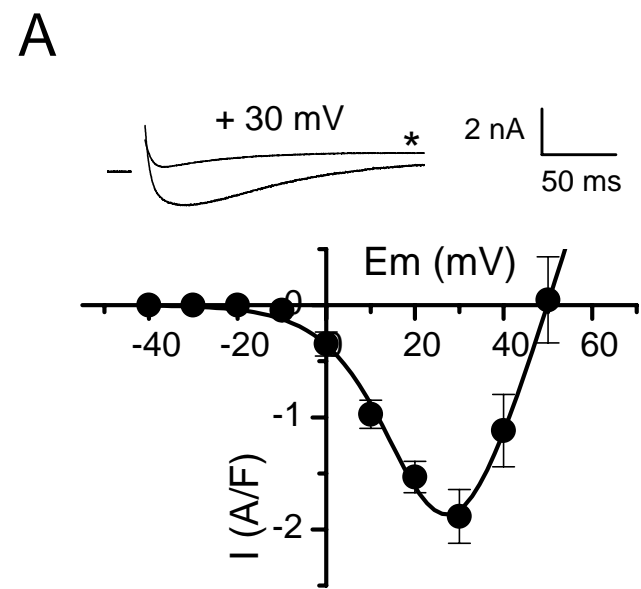


Figure 7